Spatial structure of the viscous boundary layer in turbulent convection

Xin-Liang Qiu and Ke-Qing Xia*
Department of Physics, The Chinese University of Hong Kong, Shatin, Hong Kong, China
(Received 24 June 1998)

We present an experimental study of the spatial structure of the velocity field in the boundary layer region of a Rayleigh-Bénard convection cell, using water as the working fluid. Our results show that the mean flow, the shear rate, and the viscous boundary layer thickness all change significantly across the conducting horizontal surface of the cell. Moreover, the measurements reveal that the spatial structure of the velocity field in the boundary layer region does not change with the Rayleigh number, in sharp contrast with those found for the thermal boundary layers [S.-L. Lui and K.-Q. Xia, Phys. Rev. E **57**, 5494 (1998)]. The normalized velocity profiles measured at various positions in the direction of the mean flow and for different Rayleigh number are also found to have an invariant form. [S1063-651X(98)12411-X]

PACS number(s): 47.27.Te, 44.25.+f

I. INTRODUCTION

One central focus in the current studies of the hard turbulence regime in Rayleigh-Bénard convection [1,2] is to understand the true mechanism for the apparent ''2/7'' scaling of the dimensionless heat flux with the Rayleigh number. The thermal and viscous boundary layers at the conducting surfaces have been generally recognized as playing a key role in determining the efficiency of heat transport in turbulent convection and the associated scaling and statistical properties of the temperature field. Many studies have been carried out in this regard, beginning from the early days in the investigation of convective turbulence [3] and more recently with respect to the hard turbulence regime [4–7]. A natural question arising in boundary layer studies is whether they are uniform across the horizontal plates of the convection cell. The relevance of studying the horizontal position dependence of both the shear and the viscous layer thickness at the boundary to the understanding of the heat flux scaling has been pointed out by Belmonte *et al.* [8] and also by Ching [9]. Based on experimental evidence [8] that the large-scale circulation (LSC) is not able to advect the entire heat flux across the cell and the observed existence of the thermal plumes, these authors argue that in order to take into account the role played by coherent thermal structures (such as plumes) in heat transport and also satisfying the incompressibility condition at the same time, the shear rate at the boundary cannot be a constant across the horizontal plates. In his two-dimensional (2D) simulation study of the hard turbulence regime, Werne [10] also showed that both the thermal and viscous boundary layers are nonuniform across the horizontal plate. On the other hand, a constant shear has been assumed in a theoretical model aimed at explaining the hard turbulence state [4].

Recently we have made an experimental measurement on the spatial structures of the thermal boundary layer and found that the thermal layer thickness indeed varies across the horizontal plate [11]. We also found that the scaling of the thermal layer thickness with Rayleigh number Ra changes with horizontal position. It is thus highly desirable that the spatial structure of the viscous boundary layer be measured directly and be correlated with that for the thermal boundary layer. Here we report direct experimental evidence for the position-dependent shear rate and viscous boundary layer thickness.

II. EXPERIMENT

The convection cell used in the experiment has been described in detail elsewhere [12]; we mention here only its essential features. It is a cube of dimension $L=25$ cm with its upper and lower plates made of copper and its sidewall Plexiglas. The convecting fluid used was water and the operating parameters in the experiment were the same as those in Ref. [12]. The experimental technique used for the velocity measurement near the boundary layer is *dual-beam incoherent cross-correlation spectroscopy*. The technique itself and its application to velocity measurement in turbulent convection have been well documented elsewhere [13,7,14,12] and we describe here only some of its key points.

The principle of the technique is simple: It involves measuring the time for a small seed particle having a velocity v in the flow field to cross two parallel laser beams in succession. The two laser beams have different colors and are separated by a known distance ℓ ($\sim$0.1 mm). Experimentally, this transit time, or delay time, is determined from the intensity cross-correlation function

$$g_c(t)=\frac{\langle I_b(t')I_g(t'+t)\rangle}{\langle I_b(t')\rangle\langle I_g(t')\rangle}=1+\beta G_c(t), \qquad (1)$$

where I_b and I_g are the scattered light intensities from the two parallel beams and β ($\leqslant 1$) is an instrumental constant. In our experiment, the two beams are the blue light and the green light from an argon-ion laser operated under the multiline mode. Because there is no phase coherence between I_b and I_g, the function $g_c(t)$ is sensitive only to the scattering amplitude fluctuations produced by the seed particles moving in and out of the scattering volumes. Since the separation between the two laser beams is smaller than the typical size of thermal fluctuations, the associated refractive index fluc-

*Electronic address: kxia@phy.cuhk.edu.hk

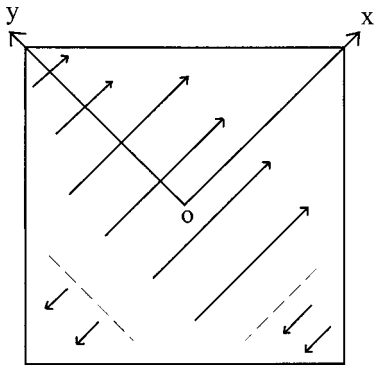

FIG. 1. Schematic drawing of the mean flow pattern near the bottom plate of the convection cell and coordinates used in our measurements. The dashed lines that demarcate the main and secondary flows are at $(-11,0)$ and $(0,-11)$, respectively.

tuations will not cause significant changes in the beam separation. With a large acceptance angle of the receiving optics, small-amplitude beam wandering in the convecting fluid will also not affect the measurement of $g_c(t)$. For a turbulent flow with the probability density function (PDF) $P(v)$ of the local velocity v assumed to be of a Gaussian, $G_c(t)$ in Eq. (1) has the form [7]

$$G_c(t)=\frac{e^{-(v_0t-\ell)^2/[r_0^2+2(\sigma t)^2]}}{N\sqrt{1+2(\sigma t/r_0)^2}}, \tag{2}$$

where r_0 is the radius of the beams, N is the average number of seeding particles in the scattering volume, and v_0 and σ are, respectively, the mean value and the standard deviation of the fluctuating velocity.

During the experiment, the convection cell sat on top of a three-dimensional translation stage (precision 0.01 mm), so that the relative position between the laser beams and the bottom plate can be easily adjusted. By fitting Eq. (2) to the measured cross-correlation function, the mean value v_0 and the standard deviation σ of the local velocity PDF $P(v)$ were obtained. It is found that the measured $G_c(t)$ at different values of Ra can all be fitted well by Eq. (2), indicating that the velocity PDF is indeed of Gaussian form as was the case in the cylindrical cell [7,14] and near the sidewall of the cubic cell [12].

III. RESULTS AND DISCUSSION

As has been found previously, the main circulation near the horizontal plates of a cubic cell is along the diagonals of the plates [15,12]. Near the corners of the cell, the flow is more complicated. As the large-scale circulation comes down along the sidewall, it produces a ''backroll'' near the corner and the horizontal shear flow near that corner is opposite to the main horizontal shear flow. Figure 1 illustrates the main and the secondary flows (separated by dashed lines) near the bottom plate of the convection cell and the coordinate system of the experiment. Note that the flow near the lower-right corner is also opposite to the main flow, which is a bit surprising as it breaks the symmetry about the mean flow.

Systematic measurements were made at both streamwise

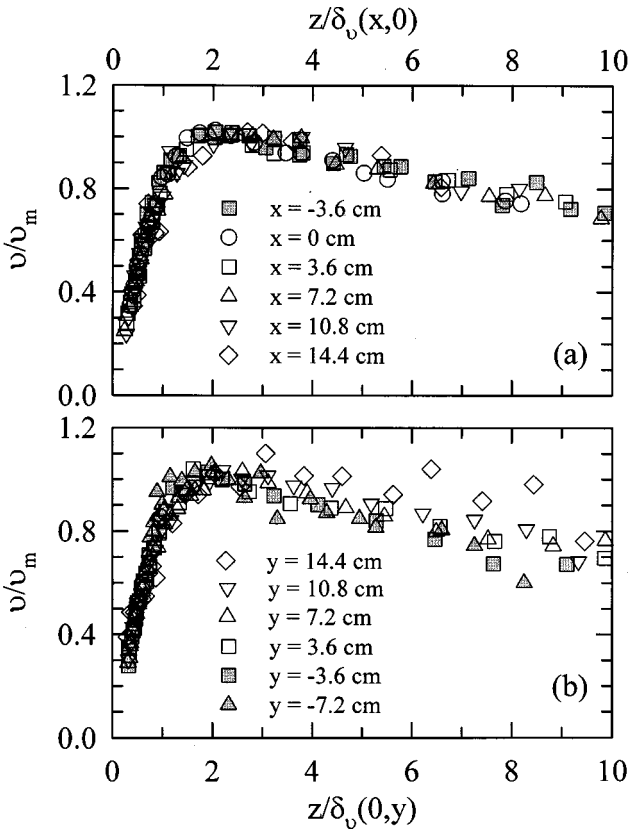

FIG. 2. Scaled mean horizontal velocity profiles as a function of the distance z from the bottom plate measured at various horizontal positions (a) along and (b) perpendicular to the LSC direction.

and spanwise positions of the main mean flow (LSC). The velocity profiles have the same general features as the ones measured at the center of the bottom plate of a cylindrical cell [7,14], i.e., they increase linearly near the plate starting from zero and after reaching a broad maximum decay towards the cell center. From the velocity profile, three boundary layer quantities can be obtained: (i) the speed of the LSC v_m (the peak value of the profile), (ii) the shear rate γ_v (which is the slope of the near-wall linear part of the profile with zero intercept), and (iii) the viscous boundary layer thickness δ_v (which is defined as the distance at which the extrapolation of the linear part of the profile equals the maximum velocity v_m or simply $\delta_v=v_m/\gamma_v$) [7,14]. We found that the profiles measured at various positions along the LSC (x axis) can all be scaled to collapse onto a single curve as shown in Fig. 2(a), where the mean horizontal velocity v is scaled by its maximum value v_m and the vertical distance z by $\delta_v(x,y)$ (due to the backroll flow in the corner of the cell, there is only one data point for $x<0$). Figure 2(b) shows the scaled profiles measured at different points along the y axis (perpendicular to the LSC). Here data are more scattered, but if the data for $y=14.4$ and -7.2 cm are taken out, then the situation will be similar to that along the LSC direction [in fact, in this case the profiles in Figs. 2(a) and 2(b) will fall onto a single curve]. From Fig. 1 we see that these positions are close to either cell corners or secondary backroll flows. This suggest that within the main flow of the LSC, velocity profiles have an invariant form. Werne's simulation showed that the velocity profiles are self-similar only within the viscous boundary layer $[z/\delta_v(x,0)<1]$ and only for upstream

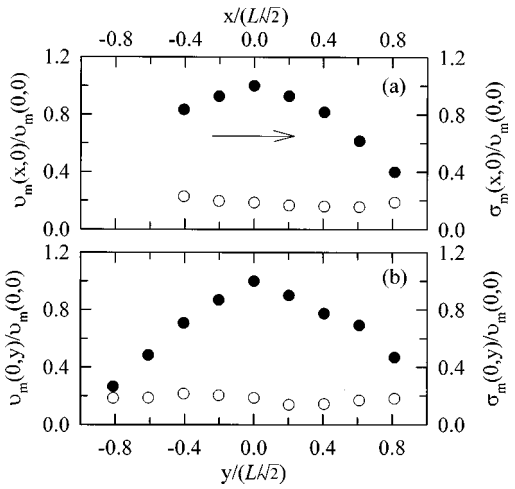

FIG. 3. Magnitude of the LSC (closed circles) measured (a) along and (b) perpendicular to the mean flow. The open circles are the corresponding rms velocities.

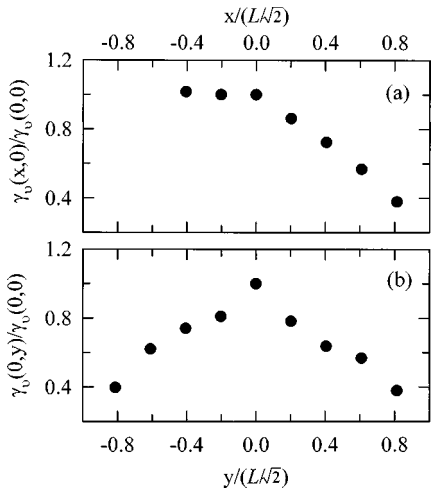

FIG. 4. Variation of the normalized shear rates (a) along and (b) perpendicular to the mean flow.

positions ($x<0$) [10]. It is clear from Fig. 2 that the invariance of the velocity profile seems to be more ''universal'' in that it extends to regions well outside the viscous boundary layer and to downstream positions ($x>0$). This result is also consistent with what was found for the temperature field [11]. We also found that mean velocity profiles measured on both the bottom plate and the sidewall [12] can be scaled to collapse onto a single curve, which implies that the above invariance of velocity profiles is not affected by whether or not a thermal boundary layer is present.

In contrast to the situation near the sidewall plate where the magnitude of the LSC and its shear near the wall are quite uniform (in the spanwise direction), the spatial variations of the same quantities over the bottom plate are substantial. Figure 3(a) shows a typical variation of the maximum mean horizontal velocity v_m (solid circles) measured along the direction of the LSC (indicated by the arrow in the figure) at $\mathrm{Ra}=3.65\times10^9$. In the figure, the horizontal axis is normalized by the half diagonal length of the bottom plate ($\mathrm{L}/\sqrt{2}$) and the vertical axis is normalized by the value of the maximum velocity at the center of the plate $v_m(0,0)$ ($=1.30$ cm/s for the present Ra). It is seen that the maximum horizontal velocity first increases with x and then decays downstream of $x=0$ after reaching a maximum at the cell center. This feature is in qualitative agreement with the numerical result of Ref. [10]. However, due to the backroll flow near the cell corner we could not observe the sharp rise of v_m in the upstream positions as found by Werne. Figure 3(b) shows the variation of v_m in the direction perpendicular to the LSC, which is a cross-sectional cut of the mean flow. Note that from the ''continuous'' profile of v_m, one would not be able to tell that the two leftmost points are actually within the secondary backroll (i.e., flow in the opposite direction), which probably is a coincidence.

The open circles in Figs. 3(a) and 3(b) are the corresponding rms values of the velocity fluctuations σ_m. It is seen that these values remain more or less constants as compared to the mean velocity. This implies that the turbulence intensity (σ_m/v_m) is the lowest in the cell center and increases toward the sidewalls. We attribute this to the interplay between the LSC and the thermal plumes in the boundary layers. Note that v_m is the peak value of the mean velocity profile, which is at the edge of the viscous boundary layer, and σ_m is the peak of the rms velocity profile. As the LSC sweeps the boundary layer and carries plumes with it, the flow in the upstream positions tends to have more cold plumes (coming down from the top to be coalesced with the hot plumes in the bottom plate) and the flow in the downstream positions tends to have more hot plumes going up (as the LSC has collected more of them on its way).

Figure 4 shows the horizontal variations of the shear rate near the viscous boundary (a) along and (b) perpendicular to the LSC (also at $\mathrm{Ra}=3.65\times10^9$ and normalized similarly as in Fig. 3). The figure reveals that shear is the strongest near the center of the horizontal plate and decays quite significantly towards the sidewall, as much as 60%. The results shown in Figs. 3 and 4 qualitatively confirm our earlier conjectures based on temperature measurement that the LSC forms a band with its magnitude and shear the strongest in the center of the band and that it also modifies the thermal boundary layer to give rise to the latter's profile [11].

Figure 5 shows the profile of the viscous boundary layer thickness $\delta_v(x,y)$ $[=v_m(x,y)/\gamma_v(x,y)]$ (a) along the mean

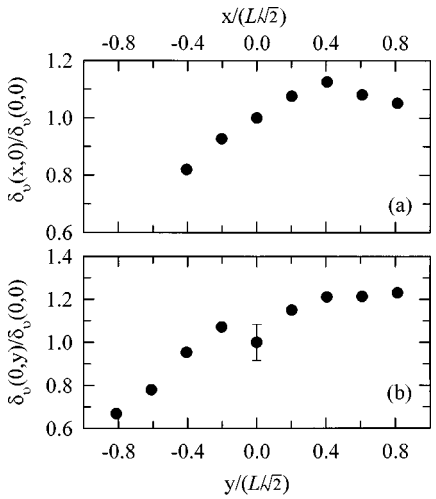

FIG. 5. Normalized viscous boundary layer thickness vs normalized position (a) in the direction of LSC and (b) perpendicular to it.

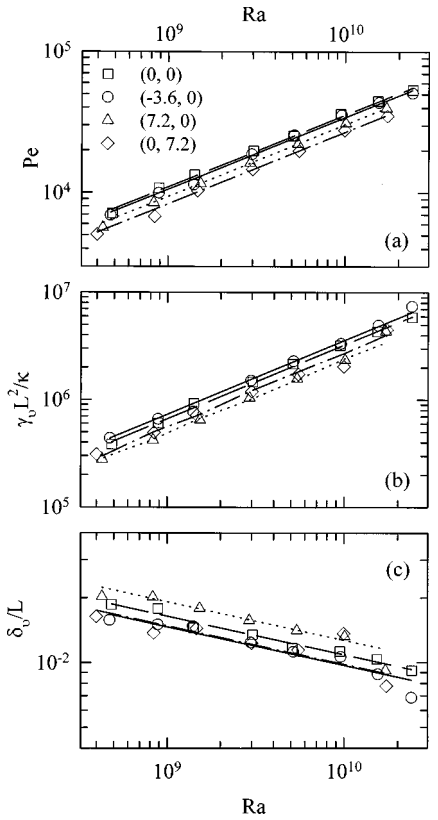

FIG. 6. (a) The Péclet number, (b) the dimensionless shear rate $\gamma_v L^2/\kappa$, and (c) the dimensionless viscous layer thickness δ_v/L as functions of Ra measured at four different positions on the bottom plate. The numbers in the parentheses to the right of the symbols are the coordinates of the positions in centimeters and are the same for all figures. See the text for the fittings.

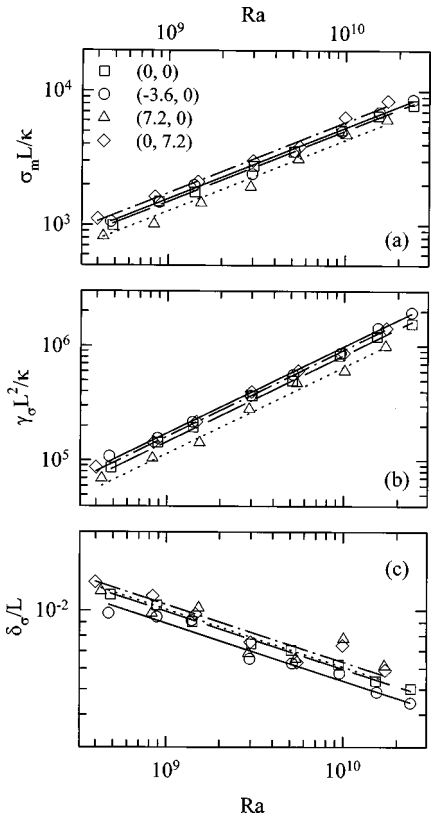

FIG. 7. Boundary layer quantities associated with the rms velocity: its maximum value σ_m, its ''shear'' γ_σ, and the length scale δ_σ, as functions of Ra measured at four different positions on the bottom plate. The symbols are the same as in Fig. 6. See the text for the fittings.

flow and (b) perpendicular to the mean flow. Again, the thickness has been normalized by its value at the center of the bottom plate $\delta_v(0,0)$ ($=3.18$ mm for the present Ra $=3.65\times10^9$) and the horizontal scale normalized by one-half of the diagonal length. Werne's simulation also shows a viscous boundary layer thickness profile that increases monotonically from the upstream corner to the downstream one [10]. The experimental and the simulation results thus share some similarities. However, unlike the simulation result, our thickness starts to decrease about midway downstream, which probably reflects the effect of the downstream sidewall. In any case, it is not realistic to expect the experiment and simulation to have detailed agreement since the two were done in different dimensions.

The horizontal variations of the various viscous boundary layer quantities as revealed by Figs. 3–5 cannot be simply explained by the sidewall effect due to the finite size of the cell. As the viscous boundary layers at the horizontal conducting plates and at the sidewall are created essentially by the same LSC, their different behavior must be primarily due to the presence of the thermal boundary layers at the conducting plates. Since a previous velocity measurement has shown that viscous boundary layer quantities are quite uniform over the sidewall plate [12], and since the mean flow across the sidewall should also experience the influence of the top and bottom plates (here playing a role similar to the one played by the sidewall with respect to flow over horizontal plates). The observed position dependence on the horizontal plates has to come mainly from the interplay between the thermal and the viscous boundary layers, as required by the vertical heat flux and the incompressibility condition.

We now look at the Rayleigh number dependence of the measured quantities. Figure 6(a) shows the Péclet number Pe ($=v_m L/\kappa$) vs Ra measured at four different positions on the bottom plate: one at the center of the plate (squares), an upstream position (circles) and a downstream one (triangles), and one away from the center of the main flow (diamonds). Figures 6(b) and 6(c) show, respectively, the nondimensional shear rate $\gamma_v L^2/\kappa$ and viscous boundary layer thickness δ_v/L as functions of Ra for the same positions as in Fig. 6(a). It is seen that the Péclet number, the shear, and the boundary layer thickness measured at different positions can all be described by respective power law fits: Pe $=(0.28,0.27,0.24,0.21)\mathrm{Ra}^{0.51\pm0.02}$, $\gamma_v L^2/\kappa=(0.41,0.45,0.30,0.34)\mathrm{Ra}^{0.69\pm0.04}$, and $\delta_v/L=(0.69,0.61,0.80,0.62)\mathrm{Ra}^{-(0.18\pm0.04)}$, where the numbers in the parentheses are for the respective positions in the order they were presented above. The fact that Pe, $\gamma_v L^2/\kappa$, and δ_v/L at different positions have the same respective Rayleigh number dependence implies that the profiles of velocity, shear, and viscous layer thickness measured along and perpendicular to the mean flow such as those shown in Figs. 3–5 will not change with Ra. The corresponding quantities of the rms velocity also exhibit similar properties and are shown in Fig.

7 where the symbols represent the same positions as they do in Fig. 6. The maximum value σ_m, the shear γ_σ, and the length scale δ_σ associated with the rms velocity are defined similarly to those for the mean velocity and are obtained from the rms velocity profile [14]. The different lines in Fig. 7 represent power law fits for data for different positions: $\sigma_m L/\kappa = (2.54, 2.67, 2.16, 3.12) \times 10^{-2} \mathrm{Ra}^{0.53 \pm 0.03}$, $\gamma_\sigma L^2/\kappa = (2.09, 2.48, 1.65, 2.33) \times 10^{-2} \mathrm{Ra}^{0.76 \pm 0.03}$, and $\delta_\sigma/L = (0.95, 0.85, 0.96, 1.01) \mathrm{Ra}^{-(0.22 \pm 0.04)}$, where the numbers in the parentheses are for the positions $(0,0)$, $(-3.6,0)$, $(7.2,0)$, and $(0,7.2)$, respectively. Note that the above exponents for the boundary layers quantities associated with the mean and the rms velocities are consistent with those obtained at the center of a cylindrical cell [7,14]. The results shown in Figs. 6 and 7 are in sharp contrast to the behavior of the temperature field where it is found that the thermal boundary layer thickness will change from a V-shaped profile in lower Ra to a uniform distribution in high Ra [11] and the scaling of the thermal layer thickness with Ra also changes with horizontal positions.

IV. CONCLUSION

In summary, we have measured the spatial structure of the velocity in the boundary layer region of a Rayleigh-Bénard convection cell operated in the hard turbulence regime. We have found that the magnitude of the mean flow, the shear rate, and the viscous boundary layer thickness all change significantly across the conducting horizontal plates of the cell in directions both along and perpendicular to the mean flow (LSC). These results contradict the assumption of a uniform shear made in a theoretical model of turbulent convection [4] and further support the view that heat flux are transported by both the horizontal LSC and coherent thermal objects near the boundary layers. Moreover, our experiments show that the measured spatial structure of the velocity field in the boundary layer region does not change with the Rayleigh number, in surprising contrast with those found for the thermal boundary layers [11]. The spatial structures of the velocity field (mean velocity profiles, profiles of viscous boundary layer thickness, etc.) revealed by our measurements also agree qualitatively with the results from a 2D simulation study [10].

ACKNOWLEDGMENT

We gratefully acknowledge the Hong Kong Research Grants Council for support of this work under Grant No. CUHK 319/96P.

[1] F. Heslot, B. Castaing, and A. Libchaber, Phys. Rev. A **36**, 5870 (1987).
[2] B. Castaing, G. Gunaratne, F. Heslot, L. P. Kadanoff, A. Libchaber, S. Thomae, X.-Z. Wu, S. Zaleski, and G. Zanetti, J. Fluid Mech. **204**, 1 (1989).
[3] D. B. Thomas and A. A. Townsend, J. Fluid Mech. **2**, 473 (1957); A.A. Townsend, *ibid.* **5**, 209 (1959).
[4] B. I. Shraiman and E. D. Siggia, Phys. Rev. A **42**, 3650 (1990).
[5] T. H. Solomon and J. P. Gollub, Phys. Rev. Lett. **64**, 2382 (1990); Phys. Rev. A **43**, 6683 (1991).
[6] A. Tilgner, A. Belmonte, and A. Libchaber, Phys. Rev. E **47**, R2253 (1993); A. Belmonte, A. Tilgner, and A. Libchaber, Phys. Rev. Lett. **70**, 4067 (1993).
[7] Y.-B. Xin, K.-Q. Xia, and P. Tong, Phys. Rev. Lett. **77**, 1266 (1996).
[8] A. Belmonte, A. Tilgner, and A. Libchaber, Phys. Rev. E **50**, 269 (1994).
[9] E. S. C. Ching, Phys. Rev. E **55**, 1189 (1997).
[10] J. Werne, Phys. Rev. E **48**, 1020 (1993).
[11] S.-L. Lui and K.-Q. Xia, Phys. Rev. E **57**, 5494 (1998).
[12] X.-L. Qiu and K.-Q. Xia, Phys. Rev. E **58**, 486 (1998).
[13] K.-Q. Xia, Y.-B. Xin, and P. Tong, J. Opt. Soc. Am. A **12**, 1571 (1995).
[14] Y.-B. Xin and K.-Q. Xia, Phys. Rev. E **56**, 3010 (1997).
[15] G. Zocchi, E. Moses, and A. Libchaber, Physica A **166**, 387 (1990).